ACS OMEGA

Open Access

This article is licensed under CC-BY-NC-ND 4.0

http://pubs.acs.org/journal/acsodf

Article

Effect of Compounded Aluminum Hydroxide Flame Retardants on the Flammability and Smoke Suppression Performance of Asphalt Binders

Kai Zhu, Yapeng Yang, Chenghang Lin, Qiang Wang,* Dong Ye, Haojia Jiang, and Ke Wu*

Cite This: *ACS Omega* 2024, 9, 2803−2814

Read Online

ACCESS | Metrics & More | Article Recommendations | Supporting Information

ABSTRACT: Compounded aluminum hydroxide (ATH) flame retardants have been widely used for their low cost and environmentally friendly characteristics. However, previous research lacks a systematic and comprehensive comparison. In addition, the combustion characteristics and phase characterization of asphalt binders are not taken into account either. In this work, flame retardants, for instance, APP, Sb_2O_3, ZB, and LDHs, were compounded with ATH. The flame retardant behavior, together with the smoke suppression behavior, of asphalt binders with compounded flame retardants was determined by LOI and CCT. Furthermore, mechanisms on flame retardants were investigated. It was found that ATH compounded with ZB significantly reduced the heat smoke release and suppressed the formation of toxic volatiles during asphalt combustion. This was because ATH/ZB facilitated the formation of polyaromatic structures and improved the resistance of the char layer. ATH compounded with APP showed an antagonistic effect in the limiting oxygen test because the reaction between ATH and APP inhibited and delayed the decomposition of ATH during asphalt combustion with more aluminum phosphate presenting relatively poor barrier properties produced.

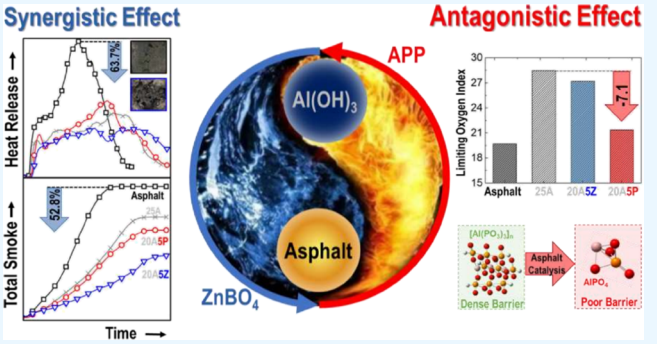

1. INTRODUCTION

Asphalt pavement, in comparison to concrete pavement, can provide a smooth, antislip, low-noise driving experience. Thanks to the rapid development of new asphalt pavement technologies, such as colored asphalt binders, noise-reducing pavement, and thin overlay technology, asphalt pavement perfectly meets the growing demand for modern tunnel pavement and thus has become the primary type of pavement in highway tunnels.[1] However, given the occurrence of fire in the tunnels, the semienclosed structural characteristics of tunnels always lead to the accumulation of heat that would not dissipate quickly. Asphalt, a flammable, high-molecular-weight material, can burn violently; temperatures can increase dramatically in a short time under heat convection and radiation. Meanwhile, a large quantity of smoke containing the toxic fumes of carbon monoxide, nitrogen oxide, and sulfur oxide would also be released during asphalt combustion. These species would be severely harmful to any persons in the affected areas.[2] Hence, the combustion inhibition of asphalt pavements is of great importance to safety risk management.

Adding flame retardants, including organic and inorganic materials, is an effective method for improving the fire resistance of asphalt.[3] Although organic flame retardants have comparable efficacy, poisonous and corrosive smoke is always emitted during combustion. It would always do harm to the environment and individuals. Inorganic metal hydroxide flame retardants, mainly presented as ATH,[4,5] MH,[6,7] HL,[8−10] and ATP,[11] are gaining increasing popularity. A large quantity of vapor produced from the decomposition of the inorganic hydroxide during the combustion process would interfere with the heat transfer process from the flame to the condensed phase of the polymer. It is consequently responsible for inhibiting the pyrolysis of the polymer and diluting the combustible gas.[1] Due to the satisfactory thermal stability of the alkaline oxides generated via decomposition, they can act as thermal insulators to reflect heat when coated onto the surfaces of the polymer. To further improve the flame retardant efficiency of inorganic metal hydroxides, it is always considered as an effective technique to have them coupled with other inorganic flame retardants.[12−16]

Decomposition of ATH generally occurs within the temperature range of 220−300 °C, which is close to that of the saturates (the most lively fraction of asphalt) combustion and lower than that of aromatics and resins (the fractions with the highest

Received: October 16, 2023
Revised: December 13, 2023
Accepted: December 15, 2023
Published: January 3, 2024

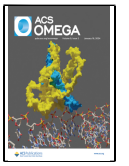

Downloaded via 49.204.141.67 on January 4, 2025 at 07:25:41 (UTC).
See https://pubs.acs.org/sharingguidelines for options on how to legitimately share published articles.

© 2024 The Authors. Published by American Chemical Society

https://doi.org/10.1021/acsomega.3c08094
ACS Omega 2024, 9, 2803−2814

Table 1. Main Properties of BA

penetration	10 °C ductility	softening point	flash point	fire point	60 °C dynamic viscosity	elemental analysis (mass ratio/wt %)				
(0.1 mm)	(cm)	(°C)	(°C)	(°C)	(× 10^3 Pa·s)	C	H	S	N	O
65.6	42.0	49.9	340	375	193	84.4	10.9	2.7	0.9	0.5

weight proportion of asphalt) combustion.[17,18] Additionally, during the asphalt combustion process, ATH also effectively inhibits the release behaviors of heat and smoke.[19,20] However, only limited high-temperature surface protection could be provided from the inert layer containing Al_2O_3 and char. Thus, the combination of ATH and flame retardants, which mainly acts in the middle and late stages in the asphalt combustion process and plays crucial roles in flame retardancy in the condensed phase, appears to be optimal.

Several researchers have investigated the effectiveness of ATH-based inorganic flame retardants. For example, given the compounding of ATH with MH, Ding et al.[5] discovered that the compounded flame retardant greatly increased the LOI and flash point of asphalt with the generation of smoke inhibited. Such effects not only enhanced the flame retardant ability of ATH in the later stages but also increased the flash point of asphalt. Huang et al.[17] found that coupling ATH with HL prolonged the TTI of the asphalt mixture and resulted in a lower heat release rate than the virgin ATH or HL. Recently, layered silicates, including OMMT and LDHs, have been added to polymer materials as the flame retardants. The resulting materials exhibited good flame retardancy and asphalt smoke suppression performance.[21] In addition, the mechanical properties of the polymer materials can also be improved by adding the previously indicated silicates. Li et al.[22] and Yang et al.[23] found the synergistic relationships between the asphalt flame retardancy and smoke suppression of the materials coupling ATH with layered silicates.

It is regrettable that previous research on ATH-based inorganic composite flame retardants still lacks a systematic and comprehensive comparison. Furthermore, the combustion characteristics and phase characterizations of asphalt binders are still essential for consideration. Owing to the different physicochemical properties and thermal decomposition reaction behaviors of flame retardants, there may be mutual catalytic effects[24] or neutralization reactions[25] in composite flame retardants. Asphalt, a complex polymer material, has a strong temperature-dependent rheology[26] and a potentially catalytic effect on flame retardants.[19,27] Therefore, it is necessary to investigate the mutual influence among the composite flame retardants and the catalytic effect of asphalt on the composite flame retardants.

Flame retardants, such as APP, Sb_2O_3, ZB, and LDHs, are the potential flame retardants to be compounded with ATH. Previous studies have indicated the use of flame retardants to inhibit pyrolysis or delay ignition.[28] APP, a typical phosphorus flame retardant, has a weight loss in 310−790 °C, covering nearly the whole temperature range of asphalt decomposition.[29] The thermal decomposition of APP produces dehydrating polyphosphate. It is able to dehydrate polymers into char and subsequently hinder heat and mass transfer. Meanwhile, released water vapor and ammonia can reduce the oxygen concentration around the combustion zone. When the content of APP increases, the flame retardancy of the composites is improved.[30] Several studies have shown that ATH and APP work well together on polypropylene (PP),[31] ethylene-vinyl acetate (EVA),[32] thermoplastic polyurethanes (TPU),[33] and epoxy resin (ER).[25] In contrast, they cause substantial damage to styrene butadiene rubber (SBR).[34] Hence, it is central to investigate the effect of ATH and APP on the behavior of asphalt binders.

Additionally, Sb_2O_3 and ZB are mainly used as effective flame retardants. Sb_2O_3, primarily operating at 475−620 °C, can generate a high-density gas adhering to the combustion surface and thus block oxygen and volatiles.[35] ZB begins to decompose at 300 °C. During this process, crystalline water could be released to lower the oxygen concentration. That would aid to form a glassy inorganic coating composed of B_2O_3 and ZnO and subsequently promote the formation of a char layer.[36] Wang et al.[37] discovered that the composite flame retardant coupling APP and ZB has a synergistic effect on the flame retardancy and smoke suppression of asphalt pyrolysis and combustion. Likewise, the thermal decomposition of LDHs usually occurs in the temperature range of 343−493 °C; the laminar structure can effectively inhibit the spreading of O_2 and heat to unburned asphalt binders. Furthermore, it also interferes with the release of combustible volatiles from the asphalt binders.[38−40] However, previous research lacks a systematic and comprehensive comparison study of composite flame retardants for the flame retardancy and smoke suppression of asphalt binders.

In this article, the flame retardancy of asphalt binders with composite flame retardants was studied and directly compared via an LOI analyzer and CCT. Then, their flame retardant mechanism was studied using the characterizations of TG-MS, XRD, and XPS. The results can provide a scientific basis for improving the flame retardancy of asphalt binders.

2. EXPERIMENTAL SECTION

2.1. Materials. BA was purchased from Bao Li Asphalt Co., Ltd. (Jiangsu, China). Table 1 presents the basic properties and elemental analysis of BA.

ZnMgAl-CO_3-LDHs (purity: 99.0%, S_{BET}: 13.2 m^2/g) were purchased from Shandong Vansinvena Material Technology Co., Ltd. (Linyi, China). ATH, APP, Sb_2O_3, and ZB were obtained from Shandong Taixing New Material Co., Ltd. The average particle sizes of ATH, APP, Sb_2O_3, ZB, and LDHs were 45, 20, 1, 7, and 2 μm, respectively.

It is reported that when the mass ratio of the ATH flame retardant to the asphalt binder is in the range of 20−25 wt %, the materials always show good flame retardant and smoke suppression performances.[22,41−43] In addition, 25 wt % is also regarded as a typical dosage of the flame retardants in polymers.[44] Therefore, in this paper, the content of the flame retardant is fixed to 25 wt %. Moreover, when the mass ratio of ATH to other flame retardants was 20:5, an excellent flame retardant performance was reported to come out.[5,45,46] For this reason, the value of this parameter in this paper was determined as 20:5. Detailed information on this is shown in the Supporting Information.

The flame retardant asphalt binders were prepared by mixing BA and the above-mentioned flame retardants using the melt blending method.[47] The detailed procedures are illustrated in our previous study.[19]

https://doi.org/10.1021/acsomega.3c08094
ACS Omega 2024, 9, 2803−2814

2.2. Test Methods and Characterizations. The LOI was tested on a YZS-8A oxygen index meter (Beijing Xinsheng Zhuorui Technology Co., Ltd.), according to ASTM D 2863-19. CCT was carried out on an FTT 0007 cone calorimeter (FTT Company, U.K.) based on ISO-5660 standard procedures under a heat flux of 50 kW/m^2. The preparation of the sample was conducted on the basis of the methods indicated in our previous study.[19] Each test was repeated three times, and the average value was calculated.

The integrated TG-MS analyzer used in this study was produced by the NETZSCH Group (Bayern, Germany). In Section 3.5, this technique was used to monitor the mass changes of the samples and the compositions of the gases during the thermal analysis process.[40,48] Approximately 10 mg of the sample was heated from room temperature to 800 °C at a heating rate of 10 °C/min in argon with a flow rate of 50 mL/min.

The XRD and XPS techniques were used to analyze the physicochemical properties of the residues after the TG-MS and CCT processes. The detailed procedures of these two characterizations are summarized in our previous study.[38] FTIR characterization was conducted on a Bruker IFS66 FTIR spectrometer at room temperature to analyze the surface functional groups of the residues.

3. RESULTS AND DISCUSSION

3.1. Limiting Oxygen Index Test. The LOI of BA is 19.7%, indicating that BA can be clearly ignited under an atmosphere of air. In contrast, the LOIs of 25A (base asphalt binder with 25% ATH) and 25P (base asphalt binder with 25% APP) are increased to 28.5 and 23.3%, respectively. This result demonstrates that the cooling effect and flame retardancy in the gaseous phase of ATH seem to be unparalleled. In the meantime, it also appears that the barrier behavior of the APP could not work satisfactorily.

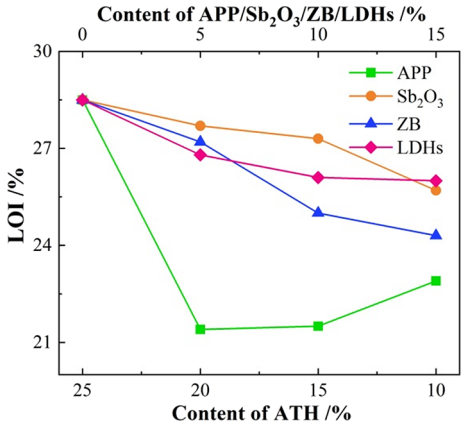

Figure 1. LOI value of asphalt binders.

The LOI curves of the asphalt binder with the partial substitution of ATH with APP, Sb_2O_3, ZB, and LDHs are shown in Figure 1. With an increase in the substitution content, the LOI of the asphalt binder decreases. This is because the LOI test method is not sensitive to the flame retardant mechanism of composite flame retardant-modified asphalt. Unexpectedly, after substituting 5 wt % ATH with APP, a significant decrease in the LOI of the asphalt binder occurs, from 28.5 to 21.4%, showing a serious antagonistic effect in the LOI test. This knowledge would be discussed in Section 3.6.

3.2. Cone Calorimeter Test. Combining the results of the LOI test and the characteristics of the flame retardant effects, APP, Sb_2O_3, ZB, and LDH flame retardants at 5 wt % were compounded with 20 wt % ATH in the cone calorimeter test. The main flammability parameters of BA, 25A, 25P, 20A5P (asphalt binder with 20 wt % ATH and 5 wt % APP), 20A5S (asphalt binder with 20 wt % ATH and 5 wt % Sb_2O_3), 20A5Z (asphalt binder with 20 wt % ATH and 5 wt % ZB), and 20A5L (asphalt binder with 20 wt % ATH and 5 wt % LDHs) are summarized in Table 2. All of these tests were repeated three times with the average values of these parameters employed.

It is seen that the TTI of 25A is 16 s. Given the replacement of 5 wt % ATH with 5 wt % APP, Sb_2O_3, ZB, and LDHs, the TTI of the asphalt binders presents a tendency of increasing. All of the HRR and THR curves of asphalt binders are illustrated in Figure 2. The HRR of BA shows a distinctive peak at 250 s. Given the introduction of flame retardants, the HRR curves of asphalt binders become broad and weak, except for that of 25P. That is to say, the HRR curve of 25P is similar to that of BA, differing only in pHRR. Compared with BA and 25P, the HRR curves of 25A, 20A5P, 20A5S, 20A5Z, and 20A5L are significantly lower, and the time corresponding to the peak HRR is somewhat longer. This finding indicates that ATH and the relevant composite flame retardants play an effective role in flame retardancy by lowering the rate of heat release. The HRR curves of 20A5L are not significantly different from those of 25A. By contrast, the curves of 20A5S and 20A5Z are located below the 25A curve until 500 s, showing good synergistic heat suppression. In particular, compared with BA and 25A, the mean HRR of 20A5Z decreases by 51.4 and 18.0%, and the peak HRR of this sample also declines by 63.7 and 23.1%.

With the increase in the combustion temperature, the barrier effect is gradually weakened after 200 s. From 200 to 430 s, the HRR value of 20A5P continues to rise and then exceeds that of 25A. In the meantime, the time for reaching the peak HRR value of the 20A5P sample is shorter than that of 25A. Therefore, the overall synergistic heat suppression effect of 20A5P is less

Table 2. Flammability Characteristics of the CCT Analysis of Asphalt Binders

		HRR/kW·m^{-2}					
samples	TTI/s	average	peak	THR/MJ·m^{-2}	EHC/MJ·kg^{-1}	TSR/10^3·m^2·m^{-2}	COY/10^{-2}·kg·kg^{-1}
BA	18 ± 2	232.3 ± 2.6	436.6 ± 4.7	110.1 ± 3.8	23.7 ± 1.4	3.73 ± 0.32	6.40 ± 0.37
25A	16 ± 3	137.5 ± 3.2	206.0 ± 5.3	83.6 ± 3.9	23.4 ± 2.1	2.87 ± 0.26	3.09 ± 0.29
25P	19 ± 4	171.3 ± 4.1	302.5 ± 6.4	82.1 ± 2.6	22.8 ± 2.8	3.22 ± 0.47	4.67 ± 0.48
20A5P	23 ± 3	137.8 ± 2.7	246.2 ± 7.8	88.1 ± 3.2	24.1 ± 2.3	2.49 ± 0.53	3.79 ± 0.31
20A5S	28 ± 4	121.2 ± 3.4	173.8 ± 3.5	84.6 ± 4.0	18.8 ± 3.0	2.56 ± 0.60	3.21 ± 0.42
20A5Z	30 ± 2	112.8 ± 2.9	158.4 ± 7.3	84.5 ± 4.3	15.1 ± 3.5	1.76 ± 0.43	2.83 ± 0.36
20A5L	32 ± 3	133.1 ± 0.5	208.5 ± 9.2	85.0 ± 0.7	17.7 ± 1.2	2.23 ± 0.23	4.45 ± 0.27

https://doi.org/10.1021/acsomega.3c08094
ACS Omega 2024, 9, 2803−2814

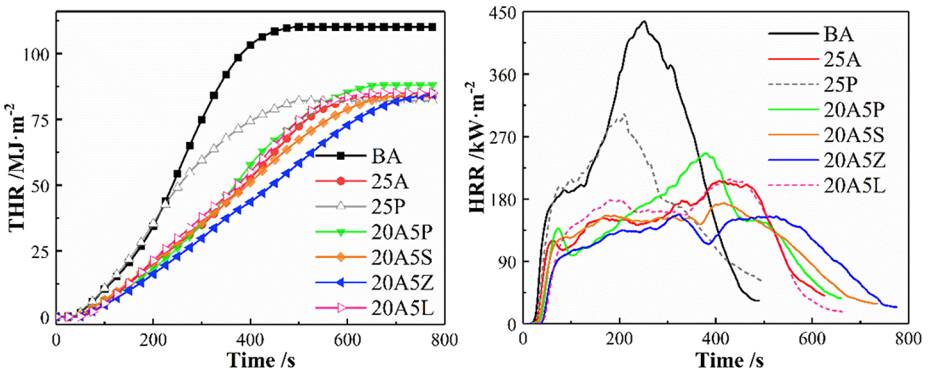

(a) THR (b) HRR

Figure 2. (a,b) Heat release of asphalt binders.

Table 3. FRI Calculation of Asphalt Binders

samples	25A	20A5P	20A5S	20A5Z	20A5L
FRI	3.72 ± 0.25	2.83 ± 0.32	5.09 ± 0.56	5.99 ± 0.47	4.82 ± 0.34

pronounced than that of the virgin 25A asphalt. This further indicates that the combination of ATH and APP has a negligible synergistic effect on the heat release performance of asphalt materials. This may be due to the fact that the asphalt substrate influences the catalytic production of additional aluminum phosphate with poor barrier characteristics. More details are provided in Section 3.6.

The mean HRR, peak HRR, and THR of 20A5P are observed to be higher than those of 25A, meaning that ATH and APP have little influence on heat release suppression. Moreover, Vahabi et al.[49] proposed a universal dimensionless standard for thermoplastic composite materials, namely, the flame retardancy index (FRI). The FRI values of all the flame retardant asphalts investigated in this article are summarized in Table 3. Within the composite flame retardant, 20A5S, 20A5Z, and 20A5L show synergistic effects, with the FRI increasing by 36.8, 61.0, and 29.6%, respectively. That is to say, 20A5Z exhibits the best flame retardant performance followed by 20A5S and 20A5L. However, 20A5P shows antagonistic effects, with the FRI declining by 23.9% compared to 25A.

All of the SPR and TSR curves of asphalt binders are shown in Figure 3. It can be seen that the asphalt binder is affected by thermal radiation in the initial stage. As a result, pyrolysis volatiles gradually accumulate, which leads to an increased SPR curve. Meanwhile, the pyrolysis volatiles are ignited and burned, which subsequently contributes to a decrease in the SPR curve. Therefore, a tiny peak will appear between 0 and 100 s. Compared with BA, the SPR value of 25P is somewhat higher in the period of 65−190 s. Such effects reveal that the admixture of APP increases the degree of precombustion of asphalt and promotes the smoke release during asphalt combustion.

The SPR of 20A5P reaches the peak value early in the combustion process, which then rapidly decreases and becomes lower than those of 25A, 20A5S, and 20A5L. This finding demonstrates that the smoke suppression of the asphalt binder is improved during this process, which reduces the degree of asphalt combustion severity. Furthermore, the SPR of 20A5Z shows the same occurrence, and its decrease is greater than that of 20A5P, which shows that the effect of ATH/ZB on smoke suppression is better than that of the ATH/APP compound. This difference can be ascribed to the fact that the ATH/ZB composite flame retardant stimulates the conversion of asphalt to char and improves the thermal oxidation resistance of the char layer. The ATH/ZB composite flame retardant also has a gas-phase flame retardant effect. It effectively inhibits the thermal resolution of asphalt composed of alkanes, olefins, benzene, and other flammable products. Additionally, the mean SPR, peak SPR, and TSR of 20A5S, 20A5Z, and 20A5L are lower than those of 25A, among which 20A5Z has the most significant synergistic smoke suppression effect. Compared to BA and 25A, the mean SPR of 20A5Z decreases by 68.8 and 41.3%,

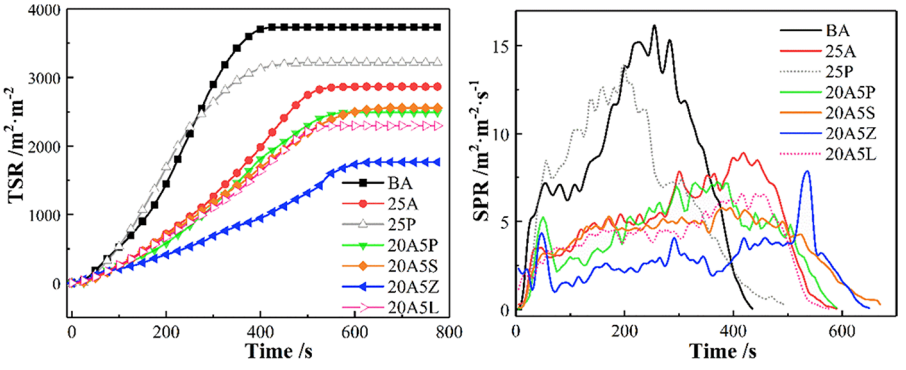

(a) Total smoke release(TSR) (b) Smoke production rate(SPR)

Figure 3. (a,b) Smoke production of asphalt binders.

https://doi.org/10.1021/acsomega.3c08094
ACS Omega 2024, 9, 2803−2814

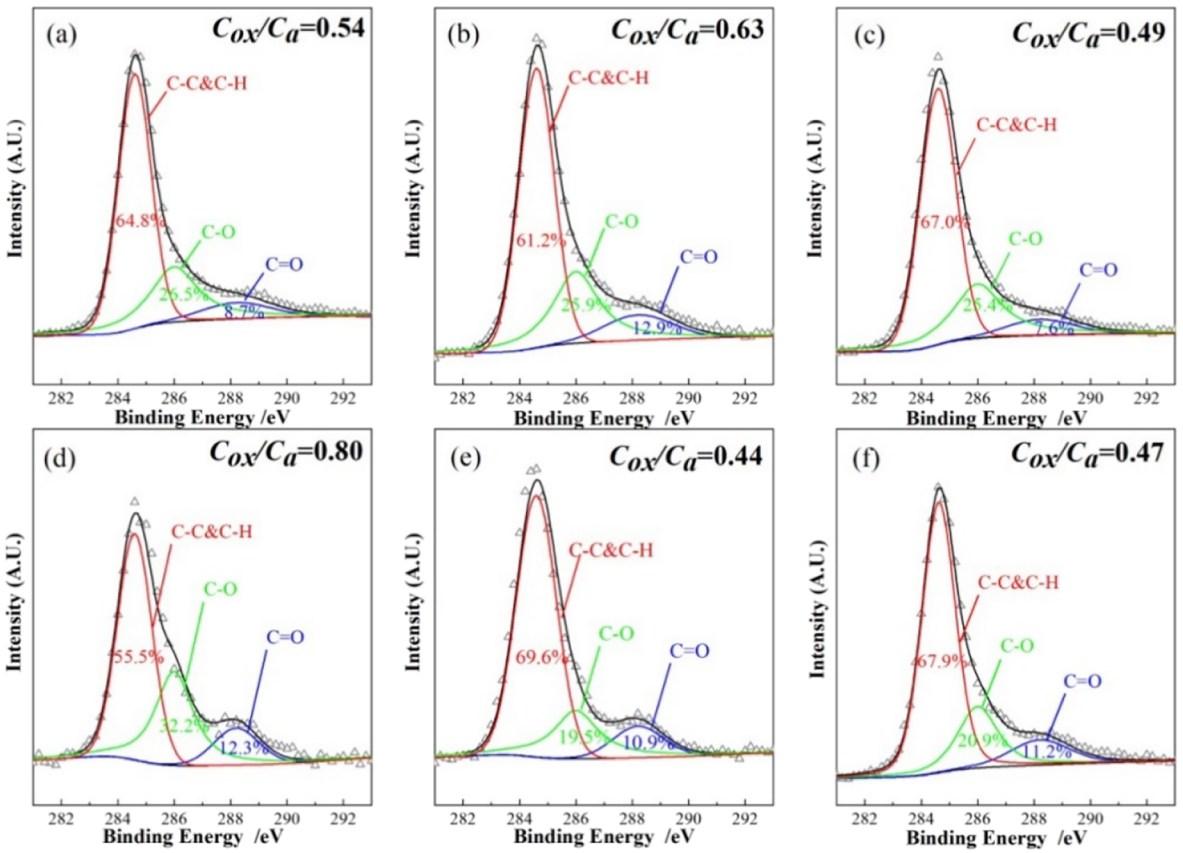

Figure 4. C 1s XPS photoelectron spectra of the residues after CCT: (a) BA, (b) 25A, (c) 20A5P, (d) 20A5S, (e) 20A5Z, and (f) 20A5L.

Table 4. Attribution of Three Subpeaks

sub-bands	C−H and C−C	C−O	C═O
attribution	aliphatic and aromatic	ether linkages	carbonyl groups

respectively. Meanwhile, a decline in the TSR by 52.8 and 38.7% also occurs for 20A5Z in comparison to BA and 25 A with the accompanying decrease in the COY by 55.8 and 8.4% (Table 2).

3.3. X-ray Photoelectron Spectroscopy Analysis. Formation of a barrier layer on asphalt binders is recognized as one of the most significant mechanisms influencing their flame retardancy. Figure 4 shows the C 1s spectra of the residues after the CCT. Through deconvolution, three sub-bands can be obtained. The attributions of these three subpeaks are shown in Table 4. C_{ox} and C_a are capable of reflecting the contents of oxidized carbons (C−O and C═O) and aromatic and aliphatic carbons (C−C and C−H), respectively. Moreover, the C_{ox}/C_a ratio was calculated to investigate the thermal oxidative resistance of the char layer.[39,50] The lower the C_{ox}/C_a ratio, the higher the C−C and C−H ratio detected in the residue. That promotes the formation of a polyaromatic structure, which is beneficial for improving the compactness and thermal oxidation resistance of the char layer.

The higher C_{ox}/C_a ratio of 20A5S than that of 25A (0.80 vs 0.63) verifies the fact that the ATH/Sb_2O_3 composite flame retardant lowers the thermal oxidation resistance. However, the C_{ox}/C_a ratio of 20A5P, 20A5Z, and 20A5L decreases to 0.49, 0.44, and 0.47, respectively. This result indicates that ATH compounded with APP, ZB, and LDHs improves the thermal oxidation resistance of the char layer. The ATH/ZB composite

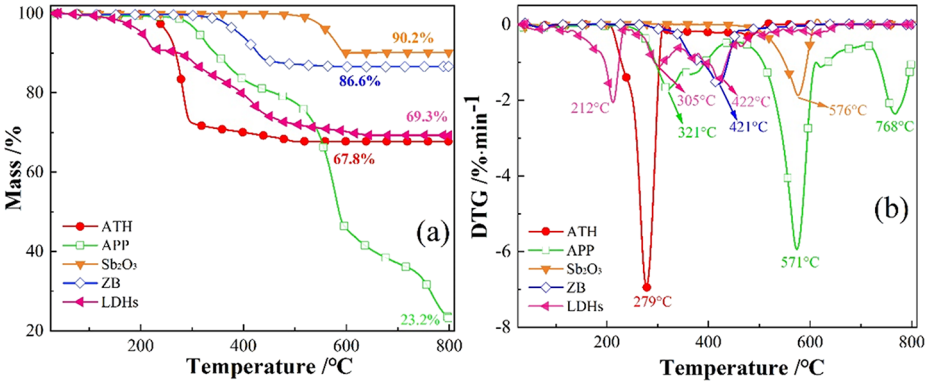

Figure 5. (a) TG and (b) DTG curves of the investigated flame retardants.

https://doi.org/10.1021/acsomega.3c08094
ACS Omega 2024, 9, 2803−2814

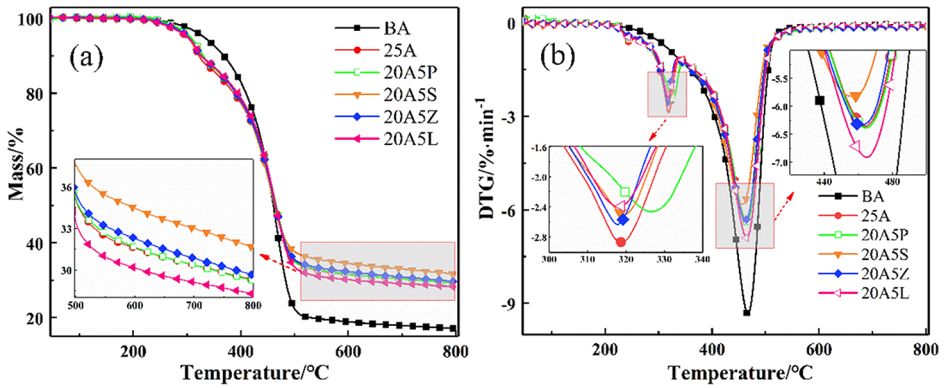

Figure 6. Thermogravimetric curves of asphalt binders: (a) TG and (b) DTG.

Table 5. Characteristic Parameters of the TG Analysis of Asphalt Binders

	stage I			stage II			
samples	temperature (°C)	peak temperature (°C)	mass loss (%)	temperature (°C)	peak temperature (°C)	mass loss (%)	residue ratio (%)
BA	265−668	468	80.9				17.1
25A	244−341	319	12.0	341−704	464	56.7	29.3
20A5P	257−350	327	12.2	350−702	465	56.5	29.3
20A5S	241−339	319	10.7	339−719	456	55.6	31.7
20A5Z	247−334	317	10.0	334−709	462	58.3	29.7
20A5L	241−336	319	10.3	336−674	464	59.4	28.3

Table 6. Identification of Released Volatile Constituents

m/z	products	*m/z*	products
16	methane (CH_4)	44	propane (C_3H_8) acetaldehyde (C_2H_4O) carbon dioxide (CO_2)
28	ethylene (C_2H_4) carbon monoxide (CO)	46	ethanol (C_2H_6O)
30	ethane (C_2H_6)	58	butane (C_4H_{10})
34	hydrogen sulfide (H_2S)	64	sulfur dioxide (SO_2)
42	propylene (C_3H_6)	78	benzene (C_6H_6)

flame retardant elevates the thermal oxidation resistance of the residue the most, explaining why 20A5Z does so well at suppressing heat and smoke release in the cone calorimeter test.

3.4. Thermal Behavior Analysis of Flame Retardants. The TG−DTG curves show the mass change of the samples, which are conducive to finding the chemical reactions of the sample at different temperature points.[51,52] Figure 5 shows the weight loss curves of ATH, APP, Sb_2O_3, ZB, and LDHs. It can be seen that the weight loss peak of ATH is centered between 227 and 314 °C. On the basis of the literature, this peak can be ascribed to the degradation of ATH after absorbing heat and releasing water vapor.[17] The mass fraction of the residue after the reaction mixture was heated to 800 °C is 67.8%. Furthermore, two weight loss peaks come out during the thermal oxidative decomposition of APP in the temperature ranges of 261−453 and 453−708 °C. These peaks are successively associated with the elimination of ammonia and water from APP to generate ultraphosphate and the fragmentation of APP to volatile P_2O_5-like moieties.[34] The weight loss peaks of Sb_2O_3 and ZB appear at 519−614 and 334−466 °C, respectively, corresponding to their sublimation and decomposition.[35] The remaining mass fractions of the two previously indicated substances after heating to 800 °C are 90.2 and 86.6%. Furthermore, LDHs have poor thermal stability, with breakdown starting at *ca.* 200 °C. The maximum decomposition rate appears at 212, 305, and 420 °C. The former two can be explained by the loss of loosely bound H_2O in the interlayer space and hydroxyl groups on the layer plates, whereas the last one is relevant to the loss of CO_3^{2-} between these layers.[39] At 800 °C, the mass fraction of the residue is 69.3%, which is similar to that of the ATH residue.

3.5. TG-MS Analysis of Asphalt Binders. Figure 6 depicts the thermogravimetric curves of asphalt binders under an argon atmosphere. Because oxygen is absent in the thermal oxidative cross-linking of asphalt, only chain-end breakage occurs. As a result, only one weight loss peak appears during the pyrolysis of BA. Both ATH and its composite asphalt binders present two weight loss peaks throughout the pyrolysis process. The first weight loss stage is the decomposition of ATH. In this stage, the decomposition of asphalt binders seems to be somehow slowed through ATH doping. The pyrolysis of asphalt binders constitutes the second weight loss process, and the peak weight loss rate is inversely connected to the thermal stability performance of asphalt binders.

Table 5 illustrates the temperature ranges and mass loss ratios in each stage. The criteria for stage division can be seen in a preliminary study.[53] It can be seen that the peak weight loss temperature of stage I of 20A5P has a significant delay compared to that of other asphalt binders, indicating that the addition of APP delays the decomposition of ATH.

In stage II, 20A5S has the lowest peak weight loss rate because Sb_2O_3 has the highest thermal stability. It starts to absorb heat at 519 °C and then begins to sublimate. Sb_2O_3 vapor with high density sinks to the vicinity of the asphalt binder burning area,[35] acting as a shield against oxygen. The peak weight loss rate of stage II of 20A5L, with a 59.4% weight loss, is significantly greater than those of other asphalt binders. It is possible that ATH simultaneously promotes the decomposition of LDHs, thus reducing the residual residue mass fraction of asphalt. In contrast, Sb_2O_3, ZB, APP, and the ATH composite all elevate the

https://doi.org/10.1021/acsomega.3c08094
ACS Omega 2024, 9, 2803−2814

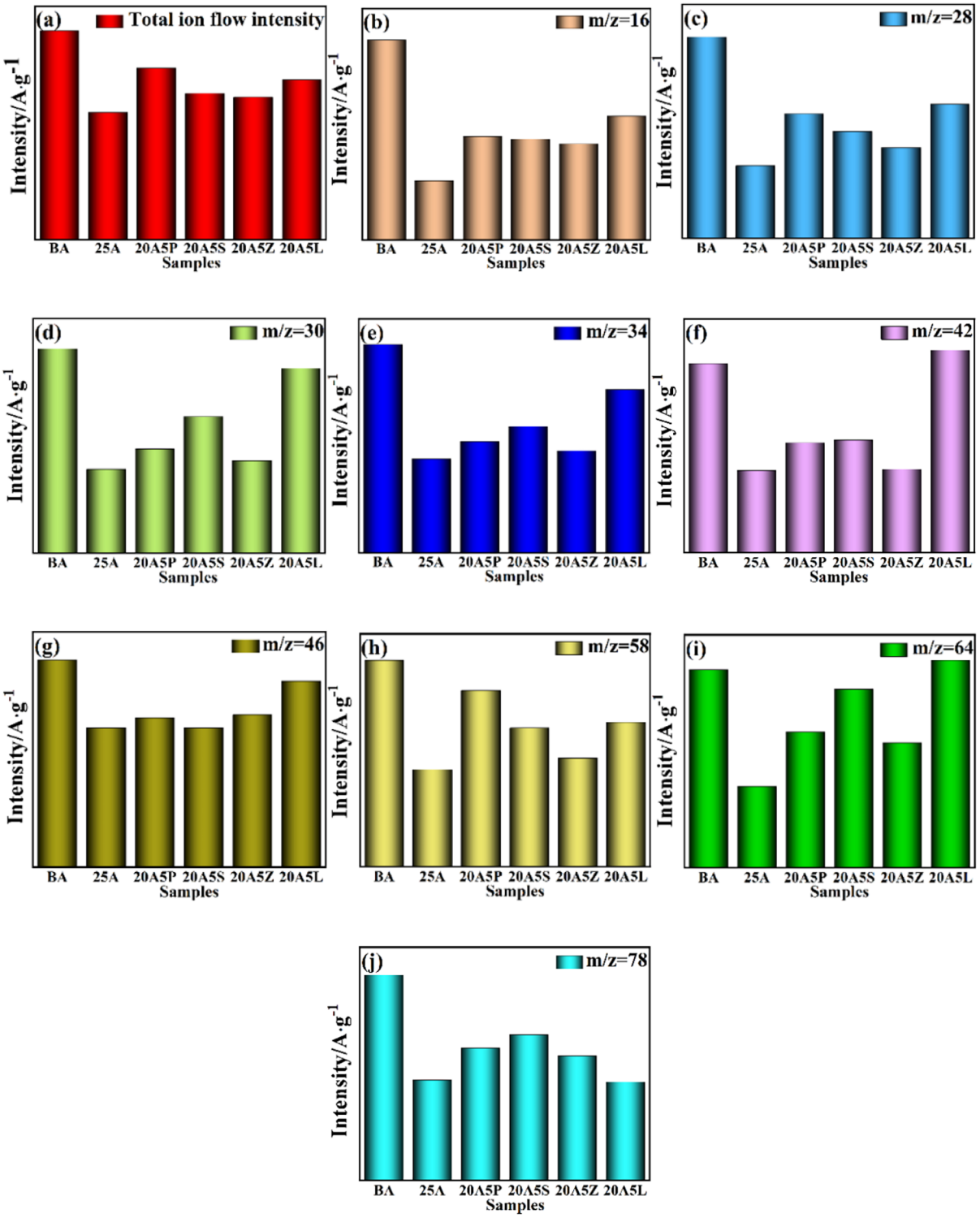

Figure 7. Peak gas release intensity for (a) total ion flow, (b) m/z = 16 CH_4, (c) m/z = 28 CO, (d) m/z = 30 C_2H_6, (e) m/z = 34 H_2S, (f) m/z = 42 C_3H_6, (g) m/z = 46 C_2H_6O, (h) m/z = 58 C_4H_{10}, (i) m/z = 64 SO_2, and (j) m/z = 78 C_6H_6.

residual residue mass fraction, among which Sb_2O_3 and ZB provide the greatest enhancement.

Since the TG-MS test was performed under an argon atmosphere, no oxygen was involved in the pyrolytic cross-linking reaction of asphalt. Therefore, the proportion of the oxygen-containing compounds produced by asphalt and asphalt binder cross-linking materials is relatively low or even negligible.

The main identified volatile constituents formed during the combustion of asphalt binders are shown in Table 6. The total ion flow intensity (a), m/z = 16 CH_4 (b), m/z = 28 CO (c), m/z = 30 C_2H_6 (d), m/z = 34 H_2S (e), m/z = 42 C_3H_6 (f), m/z = 46 C_2H_6O (g), m/z = 58 C_4H_{10} (h), m/z = 64 SO_2 (i), and m/z = 78 C_6H_6 (j) are shown in Figure 7.

From Figure 7, the peak gas release intensity of the total ion flow of 25A is the weakest. Moreover, the ability of 25A to inhibit

https://doi.org/10.1021/acsomega.3c08094
ACS Omega 2024, 9, 2803−2814

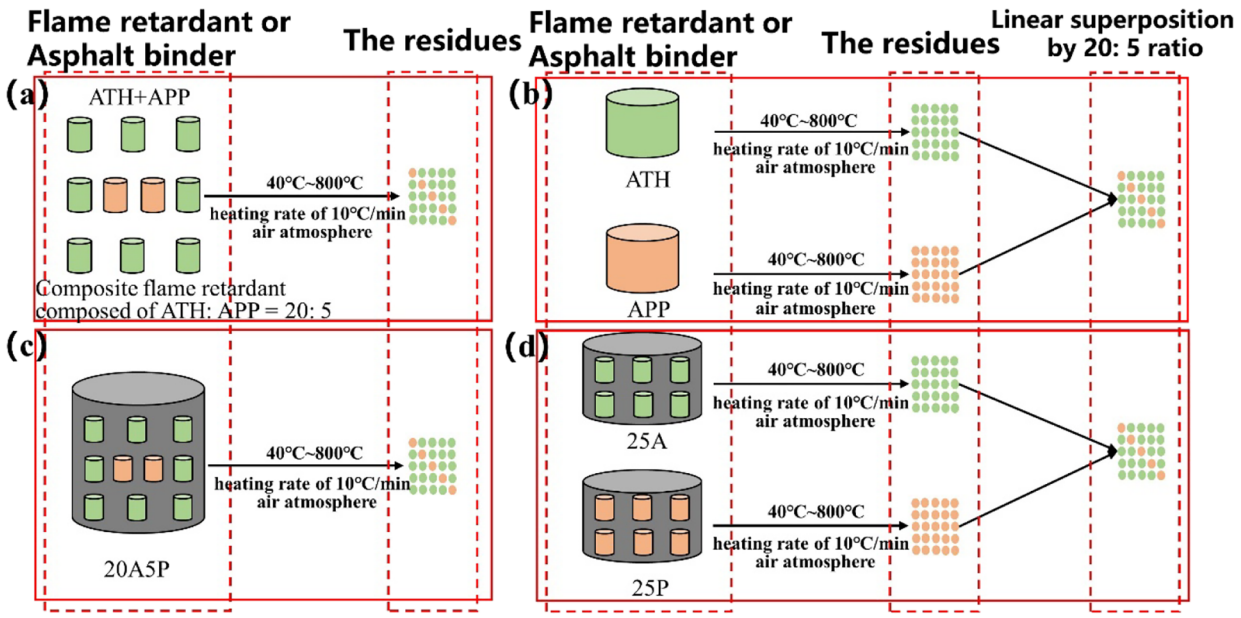

Figure 8. Schematic diagram of the mixing methods: (a) physical blending of ATH+APP, (b) linear superposition of ATH and APP, (c) physical blending of 20A5P, and (d) linear superposition of 25A and 25P.

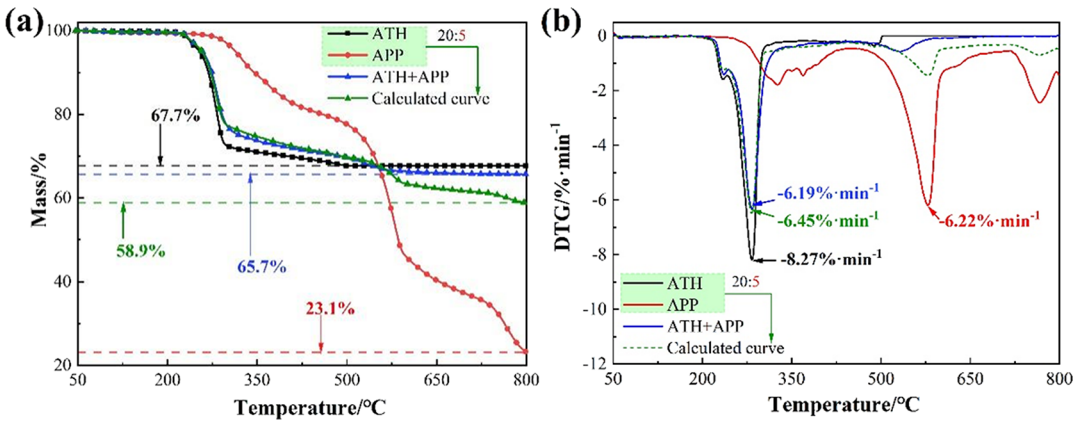

Figure 9. Thermogravimetric curves of ATH, APP, and ATH+APP and calculated curve: (a) TG and (b) DTG.

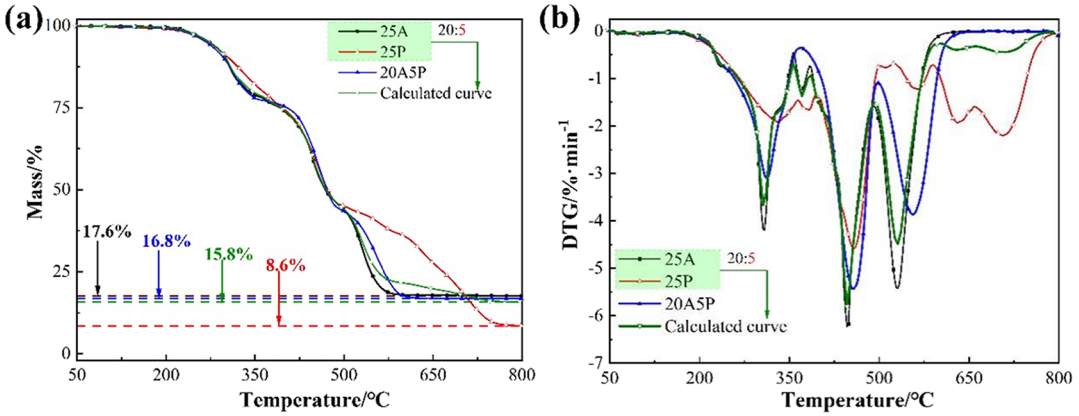

Figure 10. Comparison of the experimental and calculated curves: (a) TG and (b) DTG.

CH_4, C_2H_4, SO_2, and C_6H_6 is unparalleled. It is then replaced by 20A5Z, which stops toxic and flammable gases better in general, especially C_2H_6, C_3H_6, C_4H_{10}, and H_2S. The ability of 20A5P, 20A5S, and 20A5L to limit gas precipitation is relatively poor, with 20A5L being greater than BA in terms of the peak gas release intensity of SO_2 and C_3H_6.

3.6. Analysis of the Interaction between ATH and APP.

The compounds of ATH and APP may show synergistic or antagonistic flame retardant effects due to the influence of the

https://doi.org/10.1021/acsomega.3c08094
ACS Omega 2024, 9, 2803−2814

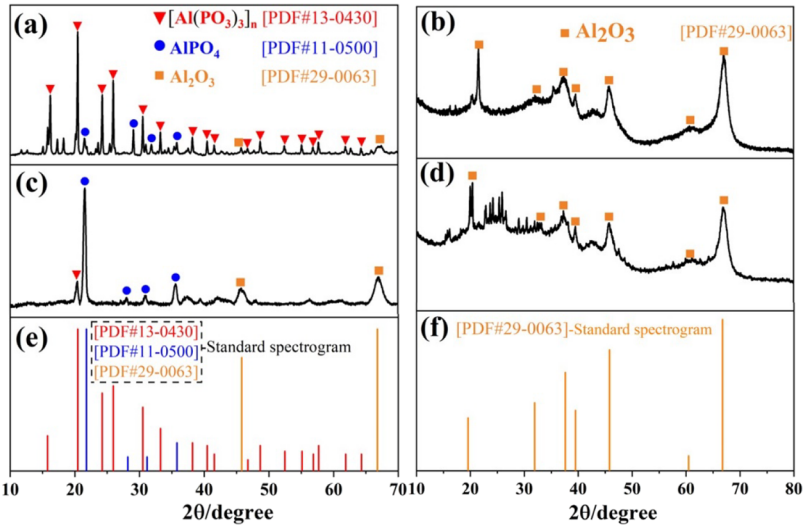

Figure 11. XRD patterns of residues of (a) ATH+APP, (b) linear superposition of ATH and APP, (c) 20A5P, (d) linear superposition of 25A and 25P, (e,f) standard spectrograms of Al_2O_3, $AlPO_4$, and $[Al(PO_3)_3]_n$.

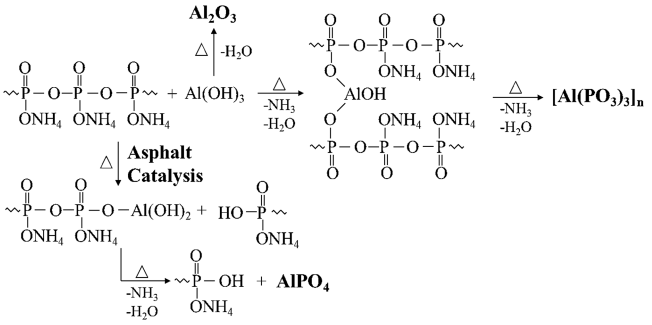

Figure 12. Possible reactions occurring between the APP and ATH.

substrate. To further analyze the role of ATH/APP in asphalt combustion, samples with different mixing methods were prepared, and the reactions of the samples were studied by the characterizations of TG and XRD.

The preparation method of the samples refers to previous studies.[32,44] The differences between the experimental and calculated curves are used to determine whether chemical reactions occur.[32,44,54] Figure 8 shows the details of the sample preparation process. On the one hand, the samples composed of ATH and APP with a mass ratio of 20:5 were heated from 40 to 800 °C under an air atmosphere at a ramping rate of 10 °C/min (Figure 8a,c). On the other hand, flame retardants or asphalt binders were separately heated at first followed by the mixing of the combustion residues (Figure 8b,d).

Figure 9 shows the thermogravimetric curves of flame retardants: ATH, APP, and ATH+APP. In addition, the thermogravimetric curves of ATH and APP linearly superimposed at a ratio of 20:5 (calculated curve) are compared with the experimental curve of ATH+APP to indicate whether chemical reactions occurred between the aforementioned two species. As shown in Figure 9a, the tested mass fraction of the residual is higher than that of the calculated one (65.7% vs 58.9%). In Figure 9b, the calculated curve has a weight loss peak at 600 °C, which cannot be observed in the experimental curve. These results demonstrate that the differences between the two aforementioned curves cannot be ignored, confirming the occurrence of the reactions between ATH and APP during the heating process. Specifically, phosphorus is converted to thermally stable substances such as aluminum phosphate and aluminum metaphosphate instead of volatile phosphide, which consequently reduces the mass loss value.

Figure 10 shows the thermogravimetric curves of asphalt binders: 25A, 25P, and 20A5P and linear superimposition of 25A and 25P at a ratio of 20:5 (calculated curve). The 20A5P has a residual mass fraction of 16.8%, which is slightly higher than that of the calculated curve. In addition, the calculated curve is similar to the DTG curve of 25A due to the different contents of ATH. The experimental curve of 20A5P is significantly distinct from the calculated curve; a decrease in the peak weight loss rate occurs for 20A5P compared with that of the calculated curve. The reductions are 15.5, 6.4, and 14.0%, further confirming the occurrence of the reaction between ATH and APP. Furthermore, the temperature of each weight loss peak is delayed by 5, 10, and 25 °C compared with that the calculated curve of 20A5P. This result indicates that APP inhibits and delays the decomposition of ATH, which explains the obvious antagonism effect between ATH and APP.

The XRD spectra of the residues are presented in Figure 11. The characteristic peaks of the residues of the mixed flame retardant and asphalt binders are identical to those of aluminum oxide.

The peaks of the residues of the composite flame retardant ATH+APP (Figure 11a) correspond to aluminum phosphate ($AlPO_4$), aluminum metaphosphate ($[Al(PO_3)_3]_n$), and aluminum oxide (Al_2O_3). Furthermore, the peak intensity of aluminum metaphosphate is observed to be greater than those of the other two species. This finding indicates that aluminum metaphosphate is dominant in the residues of ATH+APP.[55] Aluminum metaphosphate is reported as a good graphite antioxidant substance, which explains the synergistic flame retardant effect of ATH and APP in thermoplastic polymers of ER, PP, EVA, and TPU.[25,31−33] Unexpectedly, the residues of the flame retardant asphalt binder 20A5P (Figure 11c) are mainly based on aluminum phosphate ($AlPO_4$). This indicates that the reaction between ATH and APP is affected by the catalytic effect of asphalt. Subsequently, aluminum phosphate with relatively poor barrier properties is generated, which hence weakens the flame retardant effect of the condensed phase. Combining the FTIR and XPS analysis results, as we can see in

https://doi.org/10.1021/acsomega.3c08094
ACS Omega 2024, 9, 2803−2814

the Supporting Information, the possible reaction routes between APP and ATH can be summarized in Figure 12.

4. CONCLUSIONS

In this study, we investigated the effects of compounded aluminum hydroxide (ATH) flame retardants on the flame retardant and smoke suppression behaviors of asphalt binders. Some important conclusions are drawn below:

(1) The LOI of the asphalt binder is reduced via replacing 5 wt % ATH with APP, Sb_2O_3, ZB, and LDHs. Among them, the LOI of ATH compounded with APP is the lowest because the ATH−APP reaction inhibits and delays the decomposition of ATH during asphalt combustion and produces more aluminum phosphate with relatively poor barrier properties.

(2) ATH compounded with ZB and Sb_2O_3 can significantly decrease the heat release rate (HRR) of asphalt. Compared with Sb_2O_3, ZB makes pronounced impacts. The cone calorimeter tests (CCT) shows that the peak HRR decreases by 63.7 and 23.1% for 20A5Z compared with BA and 25A, respectively. This is because the ATH/ZB composite flame retardant increases the mass fraction of the carbon residue and enhances the thermal oxidation resistance of the char layer.

(3) ATH combined with ZB can reduce the release of toxic gases from asphalt combustion. The CCT indicates that compared with those of BA and 25A, the mean SPR of 20A5Z decreases by 68.8 and 41.3% with the CO yield declining by 55.8 and 8.4%. 20A5Z significantly inhibits the production of flammable gases from asphalt pyrolysis and toxic sulfur-containing compounds.

■ ASSOCIATED CONTENT

Supporting Information

The Supporting Information is available free of charge at https://pubs.acs.org/doi/10.1021/acsomega.3c08094.

(Figure S1) FTIR spectra of the residues, (Figure S2) Al 2p and P 2p XPS spectra of the residues, and (Table S1) flame retardant performances of various flame retardants (PDF)

■ AUTHOR INFORMATION

Corresponding Authors

Qiang Wang − *College of Quality and Safety Engineering, China Jiliang University, Hangzhou, Zhejiang 310018, China*; Email: qiangwang@cjlu.edu.cn

Ke Wu − *Center of Balance Architecture, Zhejiang University, Hangzhou, Zhejiang 310007, China; The Engineering Research Center of Oceanic Sensing Technology and Equipment, Ministry of Education, Zhejiang University, Zhoushan, Zhejiang 316021, China; Key Laboratory of Offshore Geotechnics and Material of Zhejiang Province, Zhejiang University, Hangzhou, Zhejiang 310058, China*; orcid.org/0000-0003-2313-3124; Email: wuke@zju.edu.cn

Authors

Kai Zhu − *College of Quality and Safety Engineering, China Jiliang University, Hangzhou, Zhejiang 310018, China; Center of Balance Architecture, Zhejiang University, Hangzhou, Zhejiang 310007, China*

Yapeng Yang − *College of Quality and Safety Engineering, China Jiliang University, Hangzhou, Zhejiang 310018, China*; orcid.org/0009-0009-8062-8909

Chenghang Lin − *College of Quality and Safety Engineering, China Jiliang University, Hangzhou, Zhejiang 310018, China; Taizhou Special Equipment Inspection and Testing Research Institute, Taizhou, Zhejiang 318000, China*

Dong Ye − *College of Quality and Safety Engineering, China Jiliang University, Hangzhou, Zhejiang 310018, China*; orcid.org/0000-0001-8299-224X

Haojia Jiang − *College of Quality and Safety Engineering, China Jiliang University, Hangzhou, Zhejiang 310018, China; Huzhou tobacco company Changxing branch, Huzhou, Zhejiang 313100, China*

Complete contact information is available at: https://pubs.acs.org/10.1021/acsomega.3c08094

Notes

The authors declare no competing financial interest.

■ ACKNOWLEDGMENTS

This work was supported by the National Natural Science Foundation of China (Grant No. 51808521), the Zhejiang Special Support Program for High-Level Personnel Recruitment of China (Grant No. 2019R52017), the Natural Science Foundation of Zhejiang Province (Grant No. LQ17E080011), and the Key Research and Development Project of Zhejiang Province (Grant No. 2018C03029).

■ NOMENCLATURE

Abbreviations

ATH	aluminum hydroxide
APP	ammonium polyphosphate
Sb_2O_3	antimony trioxide
ZB	zinc borate
LDHs	layered double hydroxides
HL	hydrated lime
MH	magnesium hydroxide
ATP	attapulgite
OMMT	organic-modified montmorillonite
BA	base asphalt
25A	asphalt binder with 25 wt % ATH
25P	asphalt binder with 25 wt % APP
20A5P	asphalt binder with 20 wt % ATH and 5 wt % APP
20A5S	asphalt binder with 20 wt % ATH and 5 wt % Sb_2O_3
20A5Z	asphalt binder with 20 wt % ATH and 5 wt % ZB
20A5L	asphalt binder with 20 wt % ATH and 5 wt % LDHs
LOI	limiting oxygen index
CCT	cone calorimeter tests
TTI	the time to ignition
HRR	heat release rate
THR	total heat release
EHC	effective heat of combustion
TSR	total smoke release
COY	carbon monoxide yield
XPS	X-ray photoelectron spectroscopy
SPR	smoke production release
TSR	total smoke release
TG	thermogravimetric
DTG	derivation thermogravimetric
MS	mass spectrometry
TG-MS	thermogravimetry and mass spectrometry

https://doi.org/10.1021/acsomega.3c08094
ACS Omega 2024, 9, 2803−2814

XRD	X-ray diffraction
FRI	flame retardancy index
S_{BET}	specific surface area

REFERENCES

(1) Xiao, F.; Guo, R.; Wang, J. Flame Retardant and Its Influence on the Performance of Asphalt − A Review. *Constr. Build. Mater.* **2019**, *212*, 841.

(2) Qiu, J.; Yang, T.; Wang, X.; Wang, L.; Zhang, G. Review of the Flame Retardancy on Highway Tunnel Asphalt Pavement. *Constr. Build. Mater.* **2019**, *195*, 468−482.

(3) Wang, H.; Yin, P. A New Flame Retardant and Its Effect on the Asphalt Mixture. *Case. Stud. Constr. Mater.* **2023**, *18*, No. e01748.

(4) Bonati, A.; Merusi, F.; Polacco, G.; Filippi, S.; Giuliani, F. Ignitability and Thermal Stability of Asphalt Binders and Mastics for Flexible Pavements in Highway Tunnels. *Constr. Build. Mater.* **2012**, *37*, 660.

(5) Ding, Q. J.; Liu, X. Q.; Shen, F.; Hu, S. G. Test and Mechanism Analysis of ATH Asphalt Flame-Retarding System. *China J. Highw. Transp.* 2008, *21* (5).

(6) Xu, T.; Huang, X.; Zhao, Y. Investigation into the Properties of Asphalt Mixtures Containing Magnesium Hydroxide Flame Retardant. *Fire Saf J.* **2011**, *46* (6), 330.

(7) Xu, T.; Huang, X. A TG-FTIR Investigation into Smoke Suppression Mechanism of Magnesium Hydroxide in Asphalt Combustion Process. *J. Anal Appl. Pyrolysis.* **2010**, *87* (2), 217.

(8) Zhu, K.; Huang, Z. Y.; Wu, K.; Wu, B.; Zhang, X.; Zhang, C. Hydrated Lime Modification of Asphalt Mixtures with Improved Fire Performance. *J. Zhejiang Univ.* **2015**, *49* (5) DOI: 10.3785/j.issn.1008-973X.2015.05.022.

(9) Little, D. N.; Petersen, J. C. Unique Effects of Hydrated Lime Filler on the Performance-Related Properties of Asphalt Cements: Physical and Chemical Interactions Revisited. *J. Mater. Civil Eng.* **2005**, *17* (2), 207.

(10) Sheng, Y.; Ahmed, A. T.; Jia, H.; Wu, Y.; Guo, P.; Li, Y.; Qiao, Y. Preparation and Characterization of Low Flammable Asphalt for Tunnel Pavements. *Constr. Build. Mater.* **2022**, *359*, No. 129559.

(11) Wang, S.; Xu, Z.; Xu, T. Improving the Controlled-Release Effects of Composite Flame Retardant by Loading on Porous Attapulgite and Coating. *Ceram. Int.* **2023**, *49* (5), 7871−7887.

(12) Wei, J. G.; Xie, C.; Fu, Q. L. Influence of Flame Retardant on Technical Performances of Asphalt and Asphalt Mixture. *China J. Highw. Transp.* **2013**, *26* (6), 30.

(13) Xia, W.; Wang, S.; Wang, H.; Xu, T. Inhibitory Effects of Developed Composite Flame Retardant on Bituminous Combustion and Volatile Emissions. *J. Clean Prod.* **2021**, *279*, No. 123538.

(14) Xia, W.; Wang, S.; Xu, T.; Jin, G. Flame Retarding and Smoke Suppressing Mechanisms of Nano Composite Flame Retardants on Bitumen and Bituminous Mixture. *Constr. Build. Mater.* **2021**, *266*, No. 121203.

(15) Chen, H.; Zheng, Z.; Guo, P.; Wang, W. Synergistic Effect of Zinc Borate on Tunnel Flame-Retardant Asphalt and Its Mechanism. *J. Build. Mater.* **2017**, *20* (4), 635.

(16) Wu, S.; Cong, P.; Yu, J.; Luo, X.; Mo, L. Experimental Investigation of Related Properties of Asphalt Binders Containing Various Flame Retardants. *Fuel.* **2006**, *85* (9), 1298.

(17) Huang, Z. Y.; Wu, B.; Kang, C.; Zhu, K.; Wu, K. Flame Retardant and Pavement Performance of Composite Hydroxide Modified Asphalt. *J. Zhejiang Univ.* 2016, *50* (1), DOI: 10.3785/j.issn.1008-973X.2016.01.005.

(18) Wang, S.; Xu, T.; Xia, W. Pyrolysis Properties of Four SARA Fractions in Asphalt. *J. Therm Anal Calorim.* **2022**, *147* (24), 14143−14153.

(19) Wu, K.; Zhu, K.; Kang, C.; Wu, B.; Huang, Z. An Experimental Investigation of Flame Retardant Mechanism of Hydrated Lime in Asphalt Mastics. *Mater. Des.* **2016**, *103*, 223.

(20) Bonati, A.; Merusi, F.; Bochicchio, G.; Tessadri, B.; Polacco, G.; Filippi, S.; Giuliani, F. Effect of Nanoclay and Conventional Flame Retardants on Asphalt Mixtures Fire Reaction. *Constr. Build. Mater.* **2013**, *47*, 990.

(21) Li, J.; Yu, J.; Wu, S.; Pang, L.; Amirkhanian, S.; Zhao, M. Effect of Inorganic Ultraviolet Resistance Nanomaterials on the Physical and Rheological Properties of Bitumen. *Constr. Build. Mater.* **2017**, *152*, 832−838.

(22) Li, M.; Pang, L.; Chen, M.; Xie, J.; Liu, Q. Effects of Aluminum Hydroxide and Layered Double Hydroxide on Asphalt Fire Resistance. *Materials* **2018**, *11* (10), 1939.

(23) Yang, X.; Shen, A.; Su, Y.; Zhao, W. Effects of Alumina Trihydrate (ATH) and Organic Montmorillonite (OMMT) on Asphalt Fume Emission and Flame Retardancy Properties of SBS-Modified Asphalt. *Constr. Build. Mater.* **2020**, *236*, No. 117576.

(24) Wang, J.; Feng, L.; Chao, X.; Feng, Y. Performance of Room Temperature Vulcanized (RTV) Silicone Rubber-Based Composites: DBDPO/RTV and DBDPE/Sb 2O 3/RTV. *Polym. - Plast Technol.* **2012**, *51* (12), 1245−1250.

(25) Liu, Y.; Tang, Z.; Zhu, J. Synergistic Flame Retardant Effect of Aluminum Hydroxide and Ammonium Polyphosphate on Epoxy Resin. *J. Appl. Polym. Sci.* **2022**, *139* (46), No. e53168, DOI: 10.1002/app.53168.

(26) Zhang, J.; Yang, F.; Pei, J.; Xu, S.; An, F. Viscosity-Temperature Characteristics of Warm Mix Asphalt Binder with Sasobit. *Constr. Build. Mater.* **2015**, *78*, 34.

(27) Petersen, J. C. A Review of the Fundamentals of Asphalt Oxidation: Chemical, Physicochemical, Physical Property and Durability Relationships", Transportation Research Circular E-C140. *ISSN* 2009.

(28) Gong, J.; Yang, L. A Review on Flaming Ignition of Solid Combustibles: Pyrolysis Kinetics, Experimental Methods and Modelling. *Fire Technol.* **2022**, *257*, No. 120487.

(29) Sheng, Y.; Wu, Y.; Yan, Y.; Jia, H.; Qiao, Y.; Underwood, B. S.; Niu, D.; Kim, Y. R. Development of Environmentally Friendly Flame Retardant to Achieve Low Flammability for Asphalt Binder Used in Tunnel Pavements. *J. Clean Prod.* **2020**, *257*, No. 120487.

(30) Javaid, A.; Hashmi, S. Development of the Fire-Retardant Truss Core Sandwich Structures Using Carbon Fiber Reinforced Epoxy Composites. *Fire Technol.* **2022**, *58* (3), 1493.

(31) Qin, Z. L.; Li, D. H.; Yang, R. J. Preparation of Ammonium Polyphosphate Coated with Aluminum Hydroxide and Its Application in Polypropylene as Flame Retardant. *J. Inorg. Mater.* **2015**, *30* (12), 1267.

(32) Lou, F.; Wu, K.; Wang, Q.; Qian, Z.; Li, S.; Guo, W. Improved Flame-Retardant and Certifiable Properties of EVA Composites by Combination of Ammonium Polyphosphate and Aluminum Hydroxide. *Polymers (Basel).* **2019**, *11* (1), 125.

(33) Peng, J. W.; Xiao, C.; Song, Q.; Peng, Z. C.; Huang, R. Sen; Yang, Y. D.; Tang, G. Flame Retardant Mechanism Investigation of Thermoplastic Polyurethane Composite/Ammonium Polyphosphate/Aluminum Hydroxide Composites Based on Spectroscopy Analysis. *Spectrosc. Spect. Anal.* **2021**, *41* (12), 3901.

(34) Castrovinci, A.; Camino, G.; Drevelle, C.; Duquesne, S.; Magniez, C.; Vouters, M. Ammonium Polyphosphate-Aluminum Trihydroxide Antagonism in Fire Retarded Butadiene-Styrene Block Copolymer. *Eur. Polym. J.* **2005**, *41* (9), 2023.

(35) Fu, Q. L.; Wei, J. G.; Peng, W. J.; Jin, L. Performance and Flame Retardant Mechanism of Coordinated Flame Retardant Asphalt with DBDPE and Sb2O3. *China J. Highw. Transp.* 2020, *33* (2).

(36) Zhuo, J.; Xiong, Y.; Chen, G.; Guo, S. Effect of Zinc Borate/MoO3 on the Flame Retardancy and Smoke Suppression of Poly(Vinyl Chloride). *Polym. Mater. Sci. Eng.* 2015, *31* (8).

(37) Wang, S.; Tan, L.; Xu, T. Synergistic Effects of Developed Composite Flame Retardant on VOCs Constituents of Heated Asphalt and Carbonized Layer Compositions. *J. Clean Prod.* **2022**, *367*, No. 133107.

(38) Zhu, K.; Wang, Y.; Tang, D.; Wang, Q.; Li, H.; Huang, Y.; Huang, Z.; Wu, K. Flame-Retardant Mechanism of Layered Double Hydroxides in Asphalt Binder. *Materials.* **2019**, *12* (5), 801.

https://doi.org/10.1021/acsomega.3c08094
ACS Omega 2024, 9, 2803−2814

(39) Zhu, K.; Tang, D.; Huang, Y.; Wang, Q.; Wu, K. Mechanism of Flame and Smoke Retardancy of Asphalt with ZnMgAl-CO3-LDHs. *J. Build. Mater.* 2019, *22* (4), DOI: 10.3969/j.issn.1007-9629.2019.04.014.
(40) Cui, P.; Wu, S.; Xiao, Y.; Wan, M.; Cui, P. Inhibiting Effect of Layered Double Hydroxides on the Emissions of Volatile Organic Compounds from Bituminous Materials. *J. Clean Prod.* **2015**, *108*, 987.
(41) Zhu, K.; Wu, K.; Wu, B.; Huang, Z. Investigations of the Montmorillonite and Aluminium Trihydrate Addition Effects on the Ignitability and Thermal Stability of Asphalt. *J. Chem.* **2014**, *2014* (8), 1−8.
(42) Yu, J.; Cong, P.; Wu, S. Investigation of the Properties of Asphalt and Its Mixtures Containing Flame Retardant Modifier. *Constr. Build. Mater.* **2009**, *23* (6), 2277−2282.
(43) Yang, X.; Wang, G.; Liang, M.; Yuan, T.; Rong, H. Effect of Aluminum Hydroxide (ATH) on Flame Retardancy and Smoke Suppression Properties of SBS-Modified Asphalt. *Road Mater. Pavement.* **2023**, *24* (1), 173−190.
(44) Wang, Y.; Zhang, L.; Yang, Y.; Cai, X. Synergistic Flame Retardant Effects and Mechanisms of Aluminum Diethylphosphinate (AlPi) in Combination with Aluminum Trihydrate (ATH) in UPR. *J. Therm Anal Calorim.* **2016**, *125* (2), 839−848.
(45) Barral, M.; Garmendia, P.; Muñoz, M. E.; Palmillas, Z.; Romera, R.; Santamaria, A.; Villanueva, S. Novel Bituminous Mastics for Pavements with Improved Fire Performance. *Constr. Build. Mater.* **2012**, *30*, 650−656.
(46) Sain, M.; Park, S. H.; Suhara, F.; Law, S. Flame Retardant and Mechanical Properties of Natural Fibre-PP Composites Containing Magnesium Hydroxide. *Polym. Degrad. Stab.* **2004**, *83* (2), 363−367.
(47) Alam, G.; Hafeez, I.; Yaseen, G.; Nasir, M. A.; Hussain, A.; Ahmad, N. Assessing the Aging Tendency of Asphalt Binder Using a Thermal Cycler. *Int. J. Pavement. Eng.* **2022**, *23* (8), 2503.
(48) Xia, W.; Xu, T.; Wang, H. Thermal Behaviors and Harmful Volatile Constituents Released from Asphalt Components at High Temperature. *J. Hazard Mater.* **2019**, *373*, 741.
(49) Vahabi, H.; Kandola, B. K.; Saeb, M. R. Flame Retardancy Index for Thermoplastic Composites. *Polymers (Basel).* **2019**, *11* (3), 407.
(50) Xu, W.; Li, C.; Wang, G.; Wang, X. Effects of ZnMgAl Layered Double Hydroxide with Different Interlayer Anions on Flame Retardant and Smoke Suppressant of Polyurethane Elastomer. *Acta Mater. Compos. Sin.* **2017**, *34* (8), 1683.
(51) Li, K. Y.; Huang, X.; Fleischmann, C.; Rein, G.; Ji, J. Pyrolysis of Medium-Density Fiberboard: Optimized Search for Kinetics Scheme and Parameters via a Genetic Algorithm Driven by Kissinger's Method. *Energ Fuel.* **2014**, *28* (9), 6130.
(52) Huang, X.; Rein, G. Smouldering Combustion of Peat in Wildfires: Inverse Modelling of the Drying and the Thermal and Oxidative Decomposition Kinetics. *Combust. Flame* **2014**, *161* (6), 1633.
(53) Zhu, K.; Qin, X.; Wang, Y.; Lin, C.; Wang, Q.; Wu, K. Effect of the Oxygen Concentration on the Combustion of Asphalt Binder. *J. Anal Appl. Pyrolysis.* **2021**, *160*, No. 105370.
(54) Castrovinci, A.; Camino, G.; Drevelle, C.; Duquesne, S.; Magniez, C.; Vouters, M. Ammonium Polyphosphate-Aluminum Trihydroxide Antagonism in Fire Retarded Butadiene-Styrene Block Copolymer. *Eur. Polym. J.* **2005**, *41* (9), 2023−2033.
(55) Vippola, M.; Ahmaniemi, S.; Keränen, J.; Vuoristo, P.; Lepistö, T.; Mäntylä, T.; Olsson, E. Aluminum Phosphate Sealed Alumina Coating: Characterization of Microstructure. *Mat Sci. Eng. A* **2002**, *323* (1−2), 1.

https://doi.org/10.1021/acsomega.3c08094
ACS Omega 2024, 9, 2803−2814